Interactions of Synoptic and Planetary Waves: Scale-Dependent Forcing of a GCM

DAVID M. STRAUS AND YUHONG YI

Center for Ocean–Land–Atmosphere Studies, Calverton, Maryland

(Manuscript received 23 July 1996, in final form 16 July 1997)

ABSTRACT

In order to better understand planetary wave–synoptic wave interactions in the atmosphere, and to develop a tool for further studies, the authors have applied a wavenumber-dependent external forcing to a general circulation model (GCM). The forcing constrains various length scales of the GCM to be close to those in the evolving analyses of the European Centre for Medium-Range Weather Forecasts and the National Centers for Environmental Prediction. The forcing acts either on the planetary waves (PW, defined as zonal wavenumbers 0–5), the synoptic waves (SW, defined as zonal wavenumbers 6–20), the synoptic waves plus the zonal mean (SW0), or the synoptic waves plus the zonal mean and wavenumber 1 (SW01). The form of the forcing is a linear relaxation to the (evolving) analyses with a time constant of 8 h. This forcing is applied only to the temperature and vorticity equations of the GCM, which has a spectral truncation of T42.

Control integrations of length 30 days have been run starting on 15 December, 1 January, and 15 January for each of the 12 winters in the period 1982/83–1993/94. This set of 36 integrations was repeated for PW forcing, SW forcing, SW0 forcing, and SW01 forcing.

The effectiveness of the SW forcing is measured by the mean zonal error variance of each wavenumber, normalized by the zonal variance in the analyses. This ratio is generally less than 0.2 when the analysis variance is large.

The systematic error of the pentad-mean 500-hPa height is very small in the PW-forced experiments compared to the control. The error reduction is very modest in the SW-forced experiments, and the zonal mean bias is *increased* compared to the control. Implications regarding errors in the GCM formulation of the planetary wave system are discussed. Dramatic reduction in the systematic error occurs only for the SW01 experiment, indicating the importance of wavenumber 1 errors in the GCM. The very modest reduction of the random pentad mean height error in the SW forced experiments compared to the control reflects the instrinsically chaotic nature of the PWs.

The 5-day mean streamfunction tendency due to bandpass transient SW–SW interactions in the control experiment tends to extend the Pacific jet too far east, and the Atlantic jet too far equatorward. The SW forcing reduces the systematic error in this transient–mean flow interaction, but systematic errors remain in the Atlantic, where the mean flow is in error. The PW-forced experiments show very low systematic error in this interaction, indicating 1) the strong steering effect of the PWs on the SWs, and 2) the ability of the GCM to simulate SWs realistically. The random error of the SW–SW transient–mean flow interaction emphasizes the intrinsic lack of predictability of the SWs.

The 5-day mean streamfunction tendency due to bandpass transient PW–SW interactions in the control experiment tends to support excessive meridional flow in the eastern Pacific, and to force the Atlantic jet too far equatorward. The reduction of the systematic error of this interaction from its value in the control experiment is marginal in the SW, SW0, and SW01 experiments, but is much greater for the PW-forced experiment, emphasizing the steering of the SWs by the mean PWs. The reduction in the random error of the PW–SW tendency from its control value is also significant for the PW-forced experiments at high latitudes.

1. Introduction

Observational studies of the large-scale low-frequency atmospheric variability have emphasized the importance of both teleconnection patterns that emerge from single-point correlations (Wallace and Gutzler 1981) and from more complex methods (Horel 1981), and the development of persistent anomalies, particularly blocking high pressure systems (Dole and Gordon 1983). Specific theoretical explanations of these phenomena have invoked the extratropical response to changes in tropical forcing (Hoskins and Karoly 1981), barotropic/baroclinic instability of the three-dimensional time-mean flow (Frederiksen 1982; Simmons et al. 1983), and transitions between large-scale multiple equilibria (Charney and deVore 1979; Charney and Straus 1980; Rambaldi and Mo 1984; LeGras and Ghil 1985; Benzi et al. 1986b). It has become clear that the mutual interactions between planetary- and synoptic-scale motions play a very large role in the evolution of the larger scales (Eg-

Corresponding author address: Dr. David M. Straus, Center for Ocean–Land–Atmosphere Studies, 4041 Powder Mill Road, Suite 302, Calverton, MD 20705-3106.
E-mail: straus@cola.iges.org

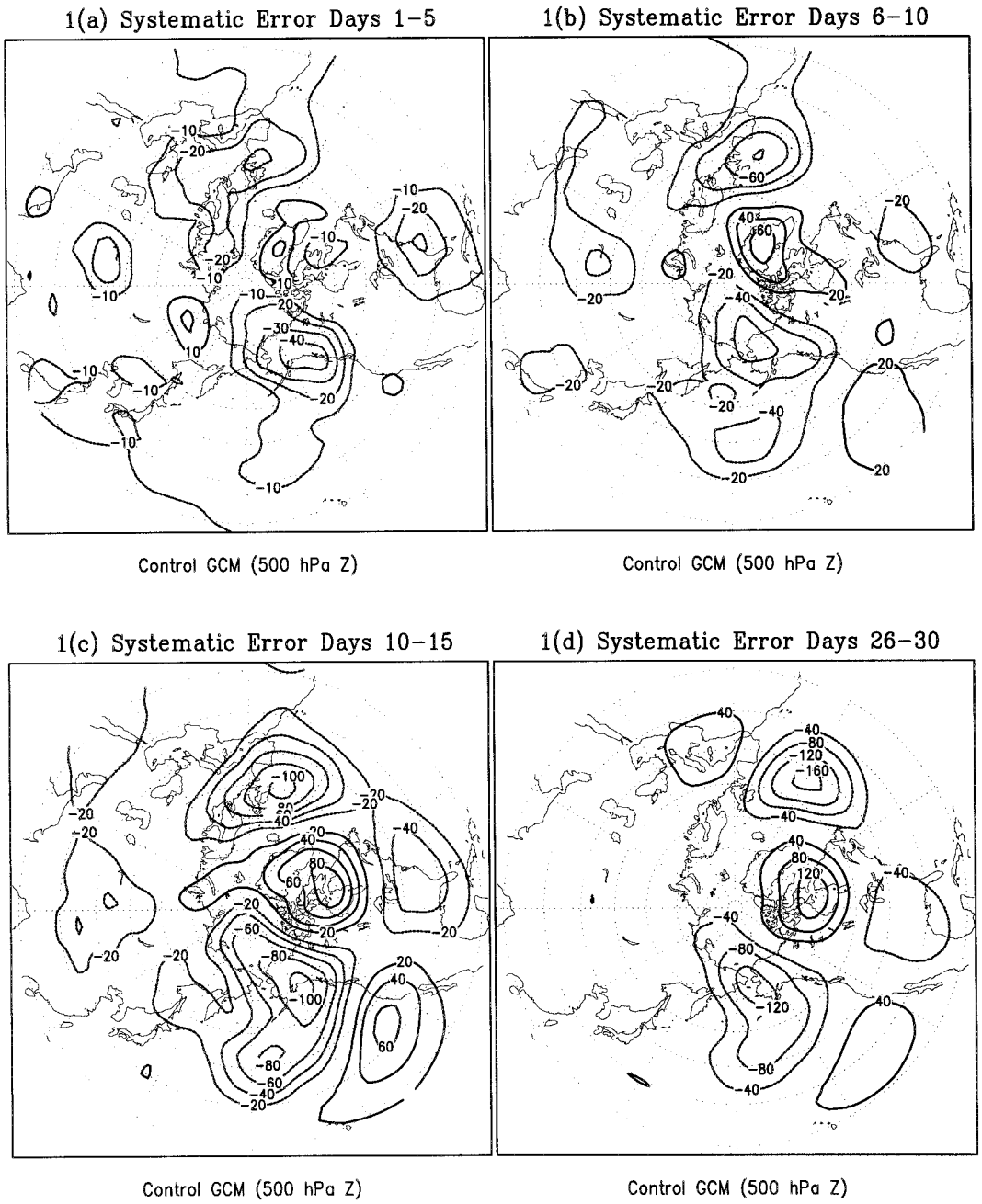

FIG. 1. Systematic error of 500-hPa height for the Northern Hemisphere from the control experiment. (a) Days 1–5. (b) Days 6–10. (c) Days 10–15. (d) Days 26–30. Contour interval is (a) 10 m, (b) and (c) 20 m, and (d) 40 m.

ger and Schilling 1983; Colucci 1985, 1987; Kung and Baker 1986; Miyakoda et al. 1986; Haines and Marshall 1987; Lau 1988; Nakamura and Wallace 1991; Tracton 1990; Tanaka 1991).

In recent years there has been a convergence of the various phenomenological concepts and theoretical ideas. The highly simplified theory of multiple equilibria has evolved into the notion of distinct large-scale regimes (Reinhold and Pierrehumbert 1982; Vautard and Legras 1988), with some support from diagnostic studies using atmospheric analyses (Benzi et al. 1986a; Hansen and Sutera 1986; Molteni et al. 1990; Cheng and Wallace 1993; Kimoto and Ghil 1993). In particular, cluster analysis of the large-scale atmospheric flow (Molteni et al. 1990; Cheng and Wallace 1993) has identified regimes in terms of discrete regions in the phase space in which the density of atmospheric states is in some sense large. These regions in phase space correspond to a combination of teleconnection patterns in physical space, and involve patterns that resemble large-

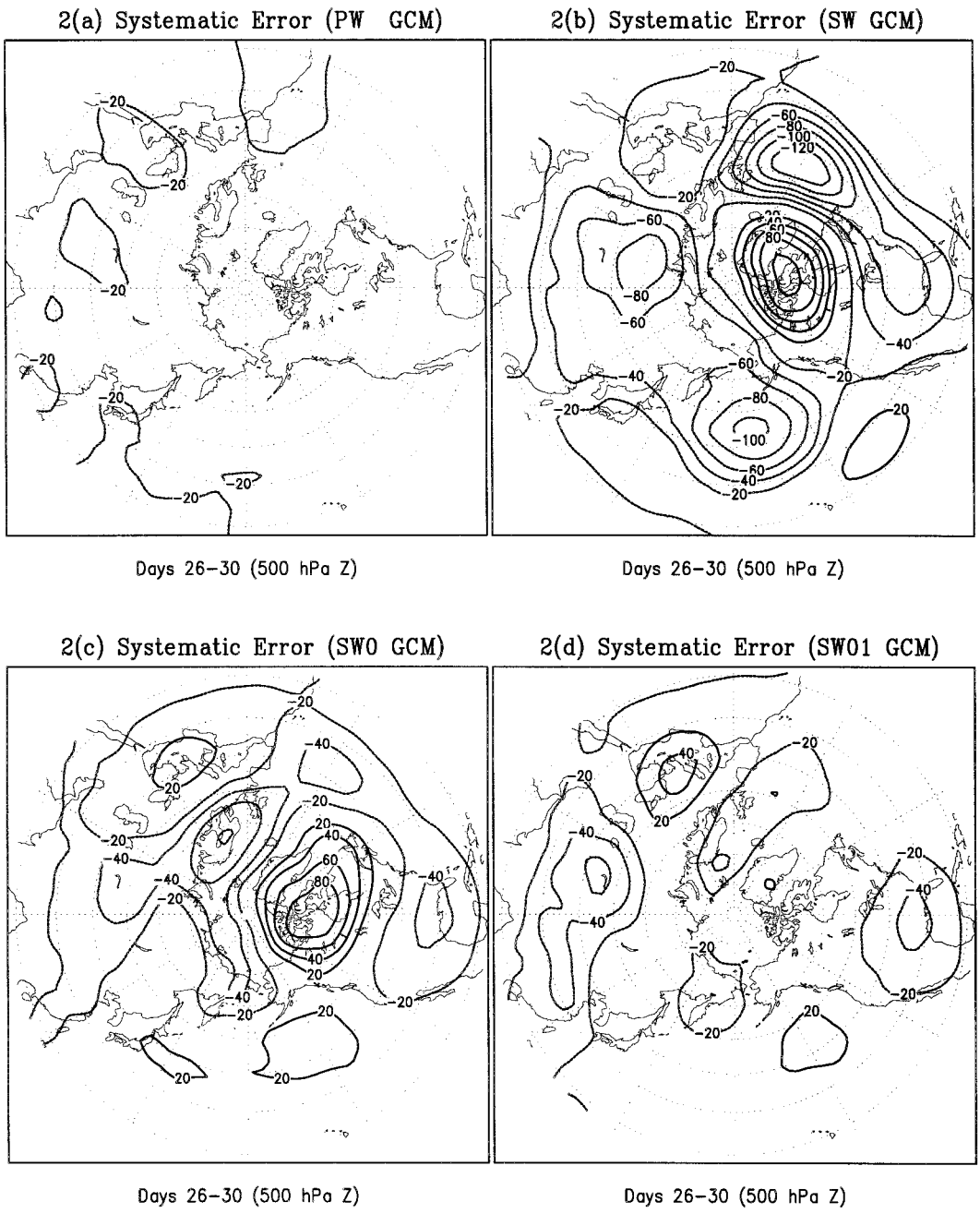

FIG. 2. Systematic error of 500-hPa height for days 26–30. (a) PW-forced experiment. (b) SW-forced experiment. (c) SW0-forced experiment. (d) SW01-forced experiment. Contour interval is 20 m.

scale blocks in certain regions. Transitions between regimes may in some cases be related to barotropic instability (Molteni and Tibaldi 1990). More generally, the interactions between synoptic and planetary scales not only play a role in these transitions (Reinhold and Yang 1993), but are intrinsic elements necessary to the existence of the regimes themselves (Reinhold and Pierrehumbert 1982; Branstator 1992). These interactions have also been shown to modulate the tropical influence on midlatitudes (Held et al. 1989).

The importance of these concepts in practical extended-range forecasting has been made quite explicit by Palmer (1988), O'Lenic and Livezey (1989), Tracton et al. (1989), Molteni and Tibaldi (1990), and Molteni and Palmer (1991). Forecast models generally have a hard time predicting the development of persistent anomalies and transitions between atmospheric regimes (Tracton et al. 1989; Palmer et al. 1990; Tibaldi and Molteni 1990). Incorrect representations of both diabatic and orographic forcing, as well as a tendency for the

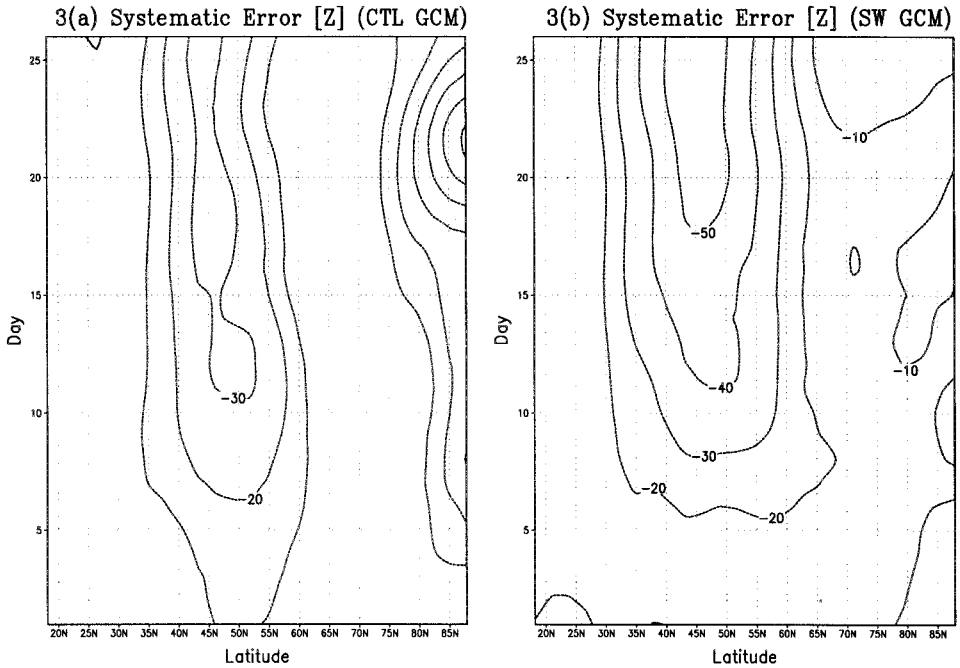

FIG. 3. Zonal mean of the systematic error in 500-hPa height as a function of time and latitude. The time labels the first day of the running-mean pentad. (a) Control experiment. (b) SW-forced experiment. Contour interval is 10 m.

model to relax strongly to its own erroneous climatology are all thought to play a role (Molteni and Tibaldi 1990).

It would be valuable to understand how forecast models handle the mutual interactions between synoptic and planetary waves in the context of transitions between different regimes, and to compare these interactions with those that occur in the atmosphere. Since these mutual interactions are so strong, diagnosis of model forecasts and comparison with analyses can only identify discrepancies. In order to understand the errors in the interactions more fully, it is necessary to be able to *specify* the evolving configuration of either the synoptic or planetary components in the model context. Detailed examination of the remaining (free) component, and of the interactions between the specified (realistic) component and the free model component would then help to understand how these interactions are (mis)represented in the model.

The purpose of this paper is to present some basic results of a method that attempts to so specify the evolving synoptic or planetary waves. We apply a linear wavenumber-dependent forcing by relaxing the planetary waves (wavenumbers 0–5, referred to as PW) and (separately) the synoptic waves (wavenumbers 6–20, referred to as SW) toward the time-dependent set of fields given by the analyses of the European Centre for Medium-Range Weather Forecasts (ECMWF) and the reanalyses of the National Centers for Environmental Prediction (NCEP) (Kalnay et al. 1996). In this paper we utilize this technique to give an overall indication of 1) how the SW components affect the slowly varying PW flow, and 2) the strength of the control exerted on the SW by the PW. We are also using the wavenumber forcing technique presented here to explore the role of scale interactions in transitions between weather regimes. That work will be reported in a separate paper.

From a physical point of view, our procedure can be compared to many earlier attempts to take into account more rapidly evolving synoptic scales in a statistical manner within the context of a model that explicitly resolves only the planetary waves (e.g., Egger and Schilling 1983). Designing such a statistical closure scheme in the case where there is strong interaction between SW and PWs is a very difficult task. In this paper, we avoid this problem by imposing the analyzed evolution of the SWs (or PWs) on the model in a brute force approach. In this procedure it is not necessary to specify the functional relationship between the SWs and PWs, and it has the advantage that the statistical behavior of the forced waves, and the relationships with the unforced waves, will be correct.

The method we use is similar to techniques that have been used in a variety of contexts. Davies and Turner (1977) investigated different linear approaches to forcing the fields in a shallow water model toward prespecified time-dependent data that were interpreted as observations. The types of forcing included both simple relaxation toward the time-dependent observations, and diffusion of the model error. Variations of this technique are sometimes referred to as dynamic relaxation, Newtonian relaxation, or nudging (Daley 1991), and have been used in the context of the hydrologic cycle (Krishnamurthi et al. 1988) and in research on

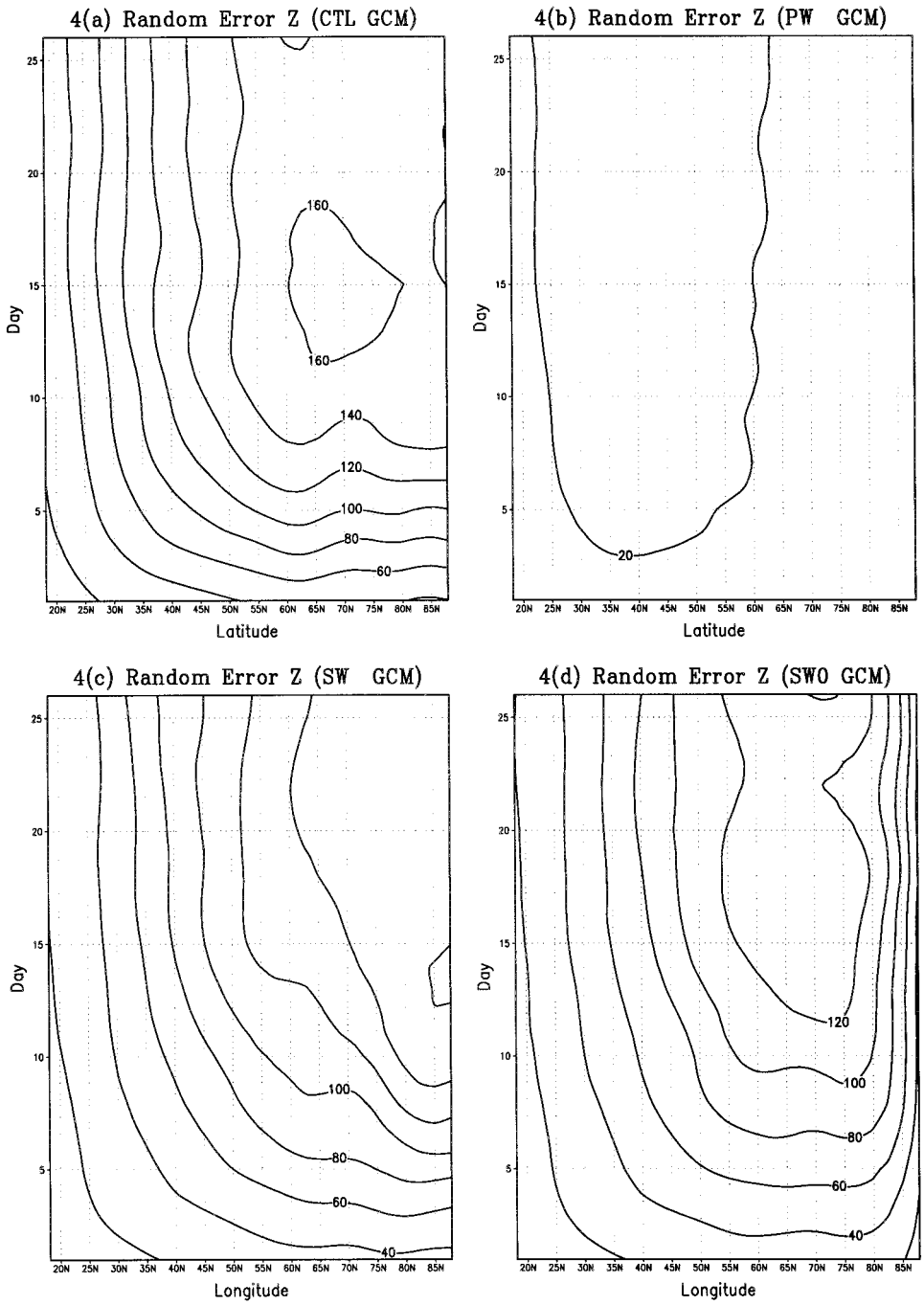

FIG. 4. Zonal mean of the random error in 500-hPa height as a function of time and latitude. The random error squared was averaged over longitude, and the square root taken. The time labels the first day of the running mean pentad. (a) Control experiment. (b) PW-forced experiment. (c) SW-forced experiment. (d) SW0-forced experiment. (e) SW01-forced experiment. Contour interval is 20 m.

improving operational forecast–analysis systems (Macpherson 1991; Bloom et al. 1996). Klinker (1990) used this type of linear forcing in an investigation of the causes of the systematic error of the general circulation model (GCM) of the ECMWF. One of the main goals was to isolate the effects of error propagation from the Tropics on the midlatitude simulation from the in situ midlatitude effects. This was accomplished by adding terms to the GCM that strongly damped the tropical errors, thus ensuring the model reproduced the fields given by the analysis. A very similar technique was used for a somewhat different purpose by Ferranti

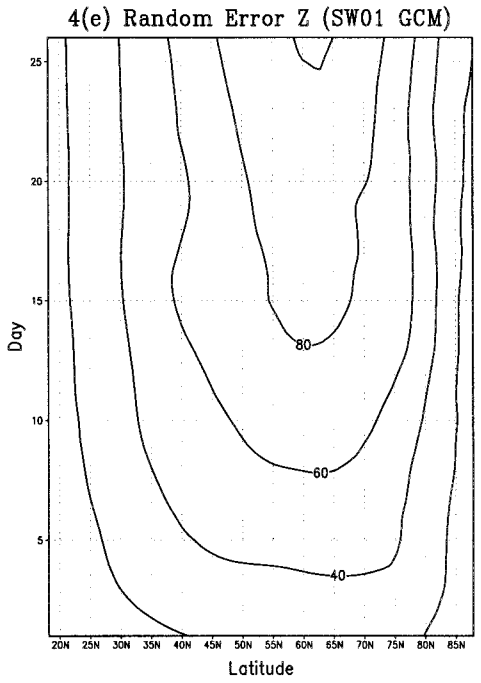

FIG. 4. (*Continued*)

et al. (1990), who were interested in the effects of the Madden–Julian oscillation (MJO) on midlatitude medium-range forecasts.

In this paper we extend this type of linear forcing into the wavenumber domain. Although superficially the forcing we use is very similar to that used in the earlier work described above, important, if subtle, differences should be noted. The previous work can be categorized either in terms of boundary value experiments (Klinker 1990; Ferranti et al. 1990), or analysis techniques, that is, establishing a balanced state consistent with the observations (Davies and Turner 1977; Daley 1991; Krishnamurthi et al. 1988; MacPherson 1991; Bloom et al. 1996). In this paper, however, we extensively examine the actual dynamical details of the flow evolution in both the forced and unforced domains. This is achieved in the context of a series of 30-day GCM forecasts, in which various components of the circulation are forced toward the evolving analyses. The mutual influence of the SWs and PWs will be probed by examining the systematic and random error components of the 5-day mean flow in a number of experiments. Each experiment consists of a set of 36 GCM forecasts of length 30 days. The experiments are distinguished by the additional forcing used, as follows: 1) no forcing (control), 2) PW forcing, 3) SW forcing, 4) SW plus zonal mean, and 5) SW plus zonal mean and wavenumber 1. The PW control of the synoptic waves will be approached by comparing the transient vorticity flux convergence due to the SW–SW and PW–SW interactions in the forced runs 2–5 above with those in the control runs.

One way of conceptualizing the forcing we use is to think of the GCM as two strongly interacting models, one for the PW system and one for the SW system. (Since the GCM utilized is a spectral model, as discussed in section 3, this concept is quite close to the reality of the model code.) Then the PW-forced integrations become integrations of the SW system in which the PWs are given by the analyses and not the PW

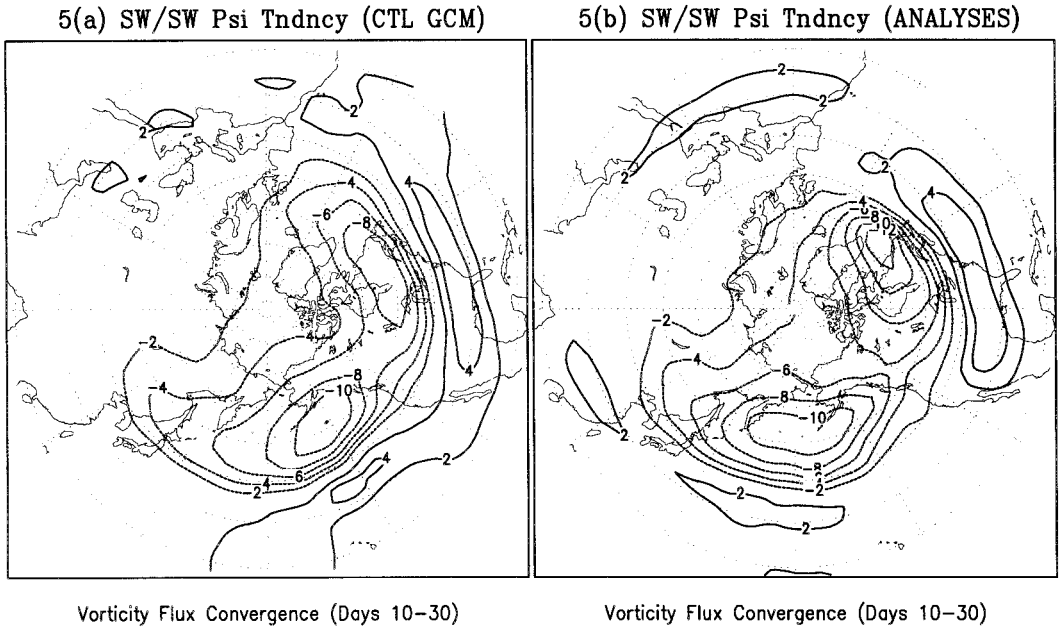

FIG. 5. Five-day mean streamfunction tendency due to SW–SW transient interactions, vertically integrated. (a) Control experiment. (b) Results from analyses. Contour interval is 2.0×10^6 m^2 s^{-1} per pentad.

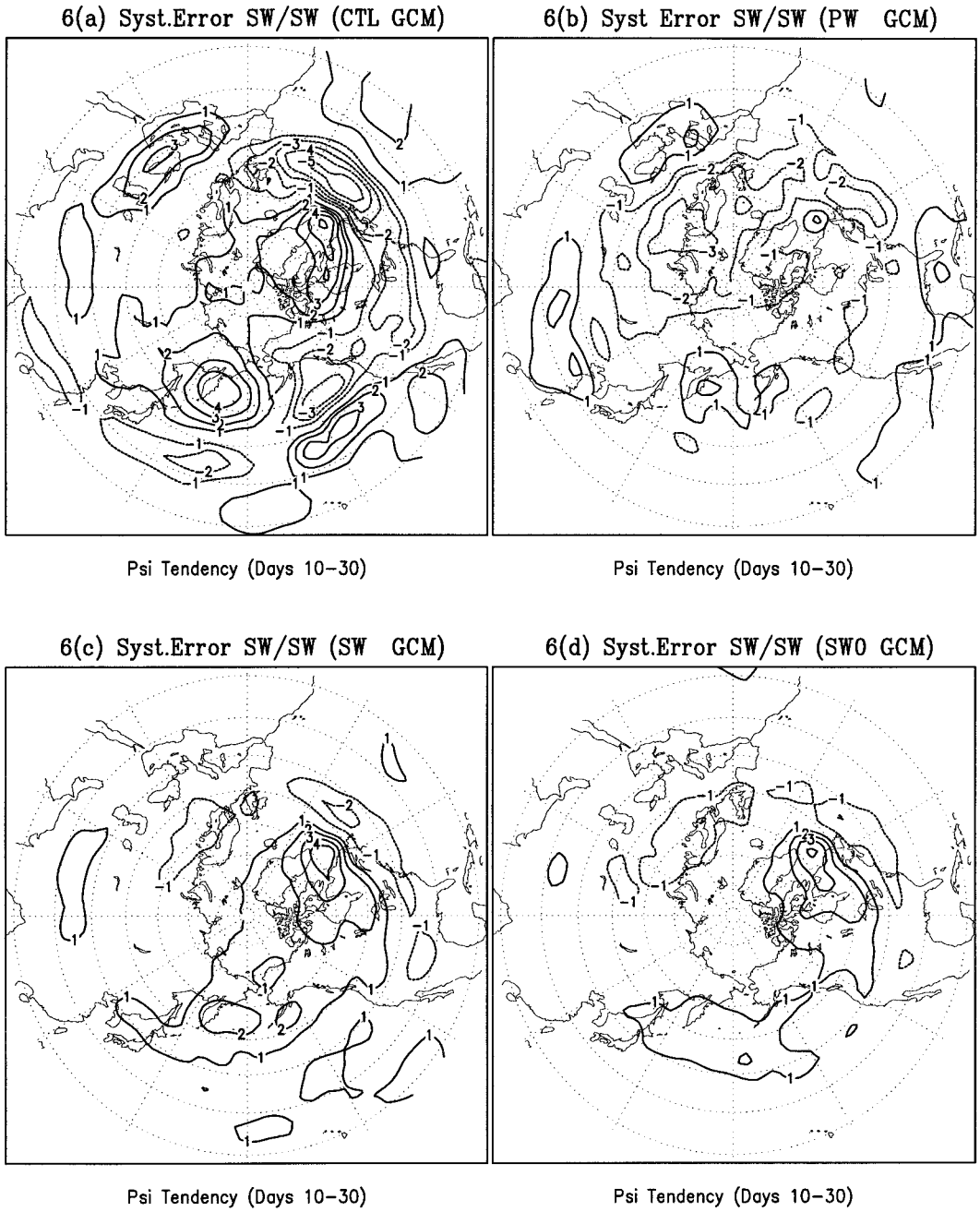

FIG. 6. Systematic error of 5-day mean streamfunction tendency due to SW–SW transient interactions, vertically integrated, for days 10–30. (a) Control experiment. (b) PW-forced experiment. (c) SW-forced experiment. (d) SW0-forced experiment. (e) SW01-forced experiment. Contour interval is 1.0×10^6 m^2 s^{-1} per pentad.

system. Similarly, the SW-forced integrations are integrations of the PW system using the analysis SWs. Similar comments apply to the other experiments.

Our approach is analogous to the work of Kushnir and Wallace (1989) in the frequency domain. They examined several forecasts in which the initial conditions were modified by removal of the high-frequency component of the circulation. By comparing the resulting behavior of the high-frequency transients with those in the control run they concluded that the configuration of these rapid transients was *not* primarily determined by that of the low-frequency fluctuations.

The plan of the paper is as follows. Details of the forcing are given in section 2. The GCM and the experiments are described in section 3, while the results for the mean flow are presented in section 4. Section 5 contains the results for the transient interactions, and a summary and discussion is given in section 6.

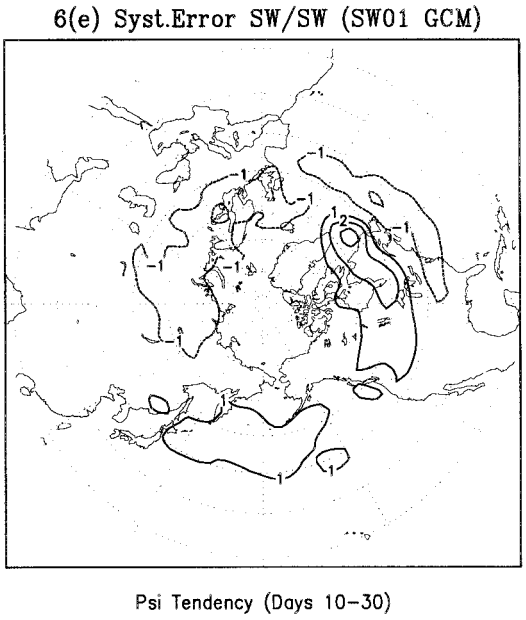

FIG. 6. (*Continued*)

2. Forcing

The basic form of the additional forcing that is added to the prognostic equations of the GCM for temperature and vorticity is

$$\frac{\partial T}{\partial t} = \cdots + \frac{1}{\tau}[T^*(t) - T(t)], \tag{1}$$

in which we choose the temperature equation for illustration. The temperature T^* to which the predicted temperature T is forced is given as follows:

$$\frac{[(t - t^{(-)})T^{*(+)} + (t^{(+)} - t)T^{*(-)}]}{[t^{(+)} - t^{(-)}]}. \tag{2}$$

Here $t^{(-)}$ and $t^{(+)}$ refer to the most recent and next analysis times, respectively, and t is the current simulated (model) time. The analysis is available every 12 h. Further, $T^{*(+)}$ and $T^{*(-)}$ refer to the corresponding analysis temperatures. The damping time τ is a constant, which is taken in our case to be 8 h, following the work of Klinker (1990). This formulation is applied to the prognostic equations for temperature and vorticity *every time step* (i.e., every 20 simulated minutes) in the GCM. In addition to temperature and vorticity, the GCM also uses divergence, specific humidity, and the log of surface pressure as prognostic variables. The forcing is actually applied in spectral space and on the GCM's vertical (sigma) surfaces, but Eq. (1) still formally applies. It is not necessary to apply the forcing to the prognostic equation for the (log of) surface pressure (Klinker 1990), and applying such a correction to the divergence field will not be effective in forcing at least the zonal-mean time average divergence (deWeaver and Nigam 1997). It turns out that our results (in midlatitudes) are very similar whether or not the forcing is applied to the divergence, so we omitted it for the experiments shown in this paper.[1] The influence of the divergence forcing on the slow planetary wave modes in the Tropics was not studied extensively.

We used the ECMWF analysis of temperature and vorticity twice daily for the winters of 1986/87–1991/92. For the winters of 1982/83–1985/86 and 1992/93–1993/94, NCEP reanalyses were used. These fields were interpolated to the model's vertical sigma surfaces, and were expressed as coefficients of spherical harmonics. This simple procedure is adequate only for relatively slowly evolving features of the atmosphere, those with a timescale of at least a day.

The modified form of (1), which includes the wavenumber dependence, is

$$\frac{\partial T_{n,m}}{\partial t} = \cdots + F_{n,m}\frac{1}{\tau}(T^*_{n,m} - T_{n,m}), \tag{3}$$

where we have made explicit the wavenumber dependence of the temperature field: n is the total (global) wavenumber and m the zonal wavenumber. The spectral quantities $T_{n,m}$ and $T^*_{n,m}$ are complex. The (real) filter $F_{n,m}$ determines which horizontal scales will be forced. In choosing this filter, the primary consideration was that the ''planetary wave'' (PW) category be able to well describe the large-scale states that characterize the regimes of the atmosphere as identified, for example, by the clusters of Cheng and Wallace (1993) or Molteni et al. (1990), and that it captures much of the signature of blocking (Tibaldi and Molteni 1990). These low-frequency structures tend to be strongly confined meridionally. In addition, we wanted the ''synoptic wave'' (SW) category to describe the transients associated with the life cycles of baroclinic waves (Simmons and Hoskins 1978), and to reflect the geographical organization of these waves in the ''storm track'' regions of the Northern Hemisphere. These considerations strongly suggest the use of *zonal* (as opposed to *total*) wavenumber to define the wave categories. While the purely geometric definition of length scales involves total wavenumber (Boer and Shepherd 1983), filtering on the basis of total wavenumber does not afford adequate discrimination on the basis of timescale and geographical organization. The baroclinic waves described by Simmons and Hoskins (1978), and their organization into storm tracks [as in Blackmon and White (1982)] are very well captured using zonal wavenumbers to define wave categories. In addition, the tight meridional confinement of persistent blocking highs is not possible to reconstruct

[1] This result may well be sensitive to both the time interval used to update the forcing (here 12 h) and the damping time τ (here 8 h). If either is much shorter, the GCM may respond more to the forcing of the divergence. The accuracy of the divergence in the analyses used to provide the forcing then becomes important.

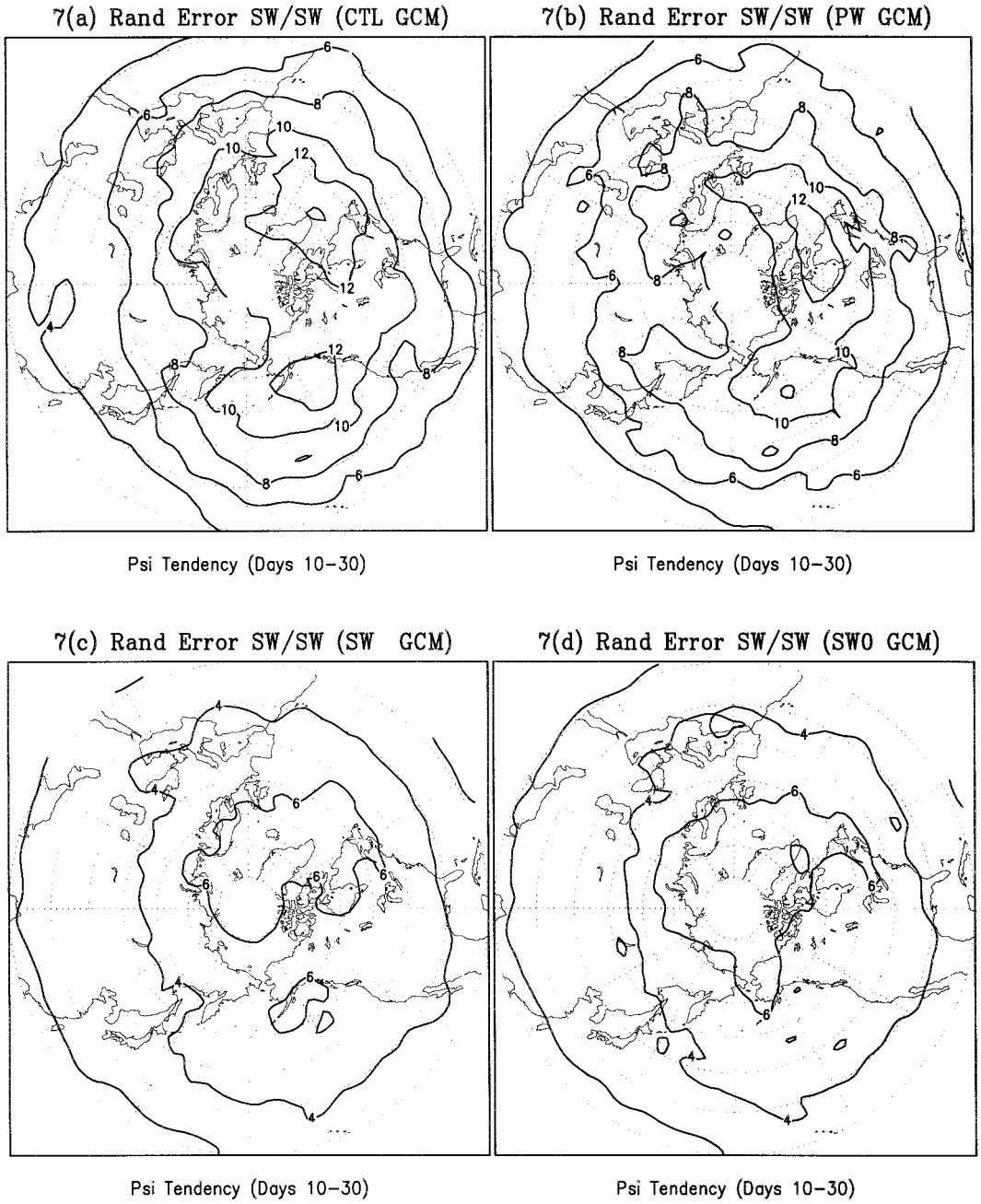

FIG. 7. Random error of 5-day mean streamfunction tendency due to SW–SW transient interactions, vertically integrated, for days 10–30. See text for details. (a) Control experiment. (b) PW-forced experiment. (c) SW-forced experiment. (d) SW0-forced experiment. (e) SW01-forced experiment. Contour interval is 2.0×10^6 m^2 s^{-1} per pentad.

using low-order spherical harmonics; a complete meridional description of the flow is needed.

The definition of the filter we used for the PW forcing is given by: $F_{n,m} = 1$ for $0 \leq m \leq 5$ (independent of n) and is otherwise 0. For the SW forcing, we take $F_{n,m} = 1$ for $6 \leq m \leq 20$ (independent of n) to be the only nonzero values. This definition of the SWs captures the energy-containing transients, but excludes very rapidly evolving small-scale features that our forcing scheme does not handle accurately. In practice a taper was applied for values of n near 20, so that F decreased gradually with increasing wavenumber.

In the appendix we discuss the degree to which the simulated amplitude and phase agree with the target amplitude and phase from the analyses. This is particularly an issue for the SW-forced integrations. Using an error measure based on the zonal variance, we show that for wavenumbers and latitudes where the SW vari-

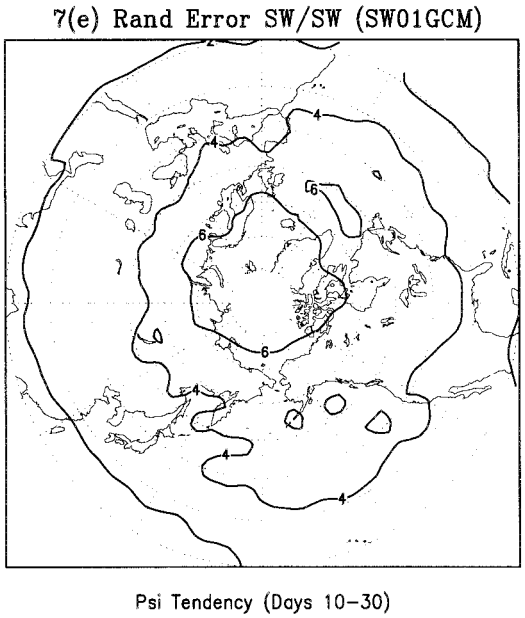

FIG. 7. (*Continued*)

ance is large, the error is less than about 20% of the analyzed variance. We also identify a mechanism by which the linear forcing can yield erroneous results. In particular, existing errors in the phase of the simulated wave can cause the amplitude to be forced incorrectly. (An extreme case would occur if the simulated wave were perfectly out of phase with the forced wave, in which case the amplitude forcing would be negative and the simulated wave would decay.) A source of phase errors for the forced waves is the nonlinear interactions with those waves not being directly forced (and hence likely to have their own errors). The forcing implied in Eq. (3) cannot damp out the phase and amplitude errors uniformly. It is possible to construct a form of the forcing that more closely accomplishes this, as we describe in the appendix. However, when expressed in terms of the spectral coefficients, this forcing is both highly nonlinear and singular.

A forcing technique that avoids these problems is incremental analysis update (IAU), as discussed in Bloom et al. 1996. In the IAU technique the model is integrated twice between times t and $t + \Delta t$ (that is, between insertions of the analysis data); once to determine the error and the second time to remove it. This is clearly more expensive computationally than the direct forcing that we have used.

The diurnal cycle is clearly misrepresented in our experiments because the interpolation is linear between analyses available only every 12 h. However, it is not expected that these errors will have any noticeable effect on the synoptic- and planetary-scale dynamics in midlatitudes above the boundary layer.

3. GCM experiments and error measures

a. GCM

The GCM utilized in this study is the GCM of the Center for Ocean–Land–Atmosphere Studies (COLA) at spectral resolution triangular 42 (T42). The prog-

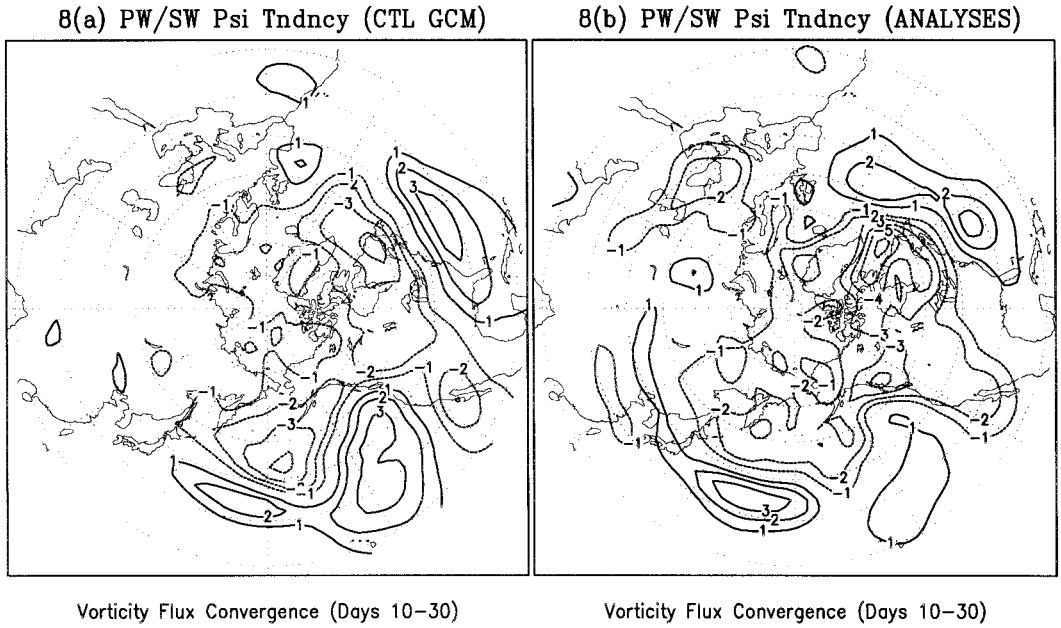

FIG. 8. Five-day mean streamfunction tendency due to PW–SW transient interactions, vertically integrated. (a) Control experiment. (b) Results from analyses. Contour interval is 1.0×10^6 m^2 s^{-1} per pentad.

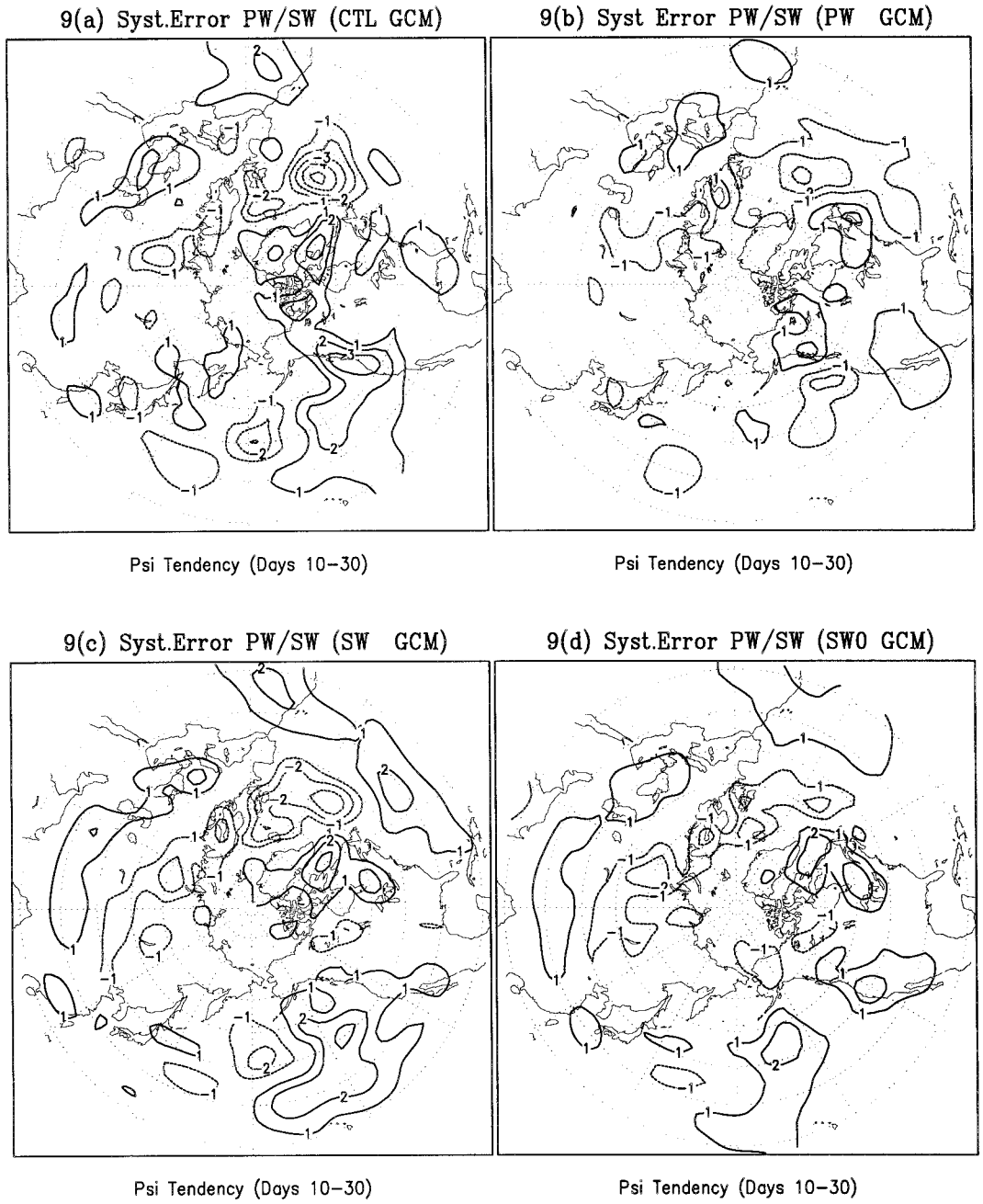

FIG. 9. Systematic error of 5-day mean streamfunction tendency due to PW–SW transient interactions, vertically integrated, for days 10–30. See text for details. (a) Control experiment. (b) PW-forced experiment. (c) SW-forced experiment. (d) SW0-forced experiment. (e) SW01-forced experiment. Contour interval is 1.0×10^6 m^2 s^{-1} per pentad.

nostic variables consist of spectral representations of temperature, vorticity, divergence, specific humidity, and the log of surface pressure. The GCM features a full suite of parameterizations, including, for example, long- and shortwave radiation, cumulus and shallow convection, large-scale latent heat release, cloud–radiation interaction, interactions with a model biosphere, and gravity wave drag (see Xue et al. 1996, and references therein).

b. Experiments

Five experiments were run, each consisting of 36 simulations of length 30 days. The set of control integrations started from analyses valid for 0000 UTC 15 December, 1 January, and 15 January for the 12 winters of 1982/83–1993/94. Observed sea surface temperatures (SSTs) and sea ice were used in all the integrations. The initial conditions were obtained from the ECMWF anal-

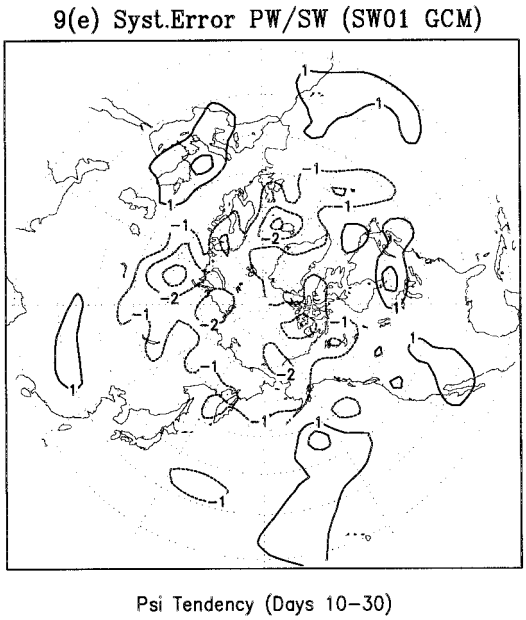

FIG. 9. (*Continued*)

yses for the last nine winters, and from the NCEP reanalyses for the first three winters. In parallel to the control experiment, four additional experiments were run that utilized the same initial conditions, SST and sea ice, but in which the forcing toward the analyses was added. In the PW experiment, zonal waves 0–5 were forced toward the analyses as described in section 2. In the SW experiment, zonal waves 6–20 were forced. In the SW0 experiment, zonal waves 0 and 6–20 were forced, and in the SW01 experiment, zonal waves 0, 1, and 6–20 were forced. Thus the zonally averaged flow was forced by the analyses in the PW, SW0, and SW01 experiments, and wavenumber 1 was forced only in the PW and SW01 experiments.

The choice of three (overlapping) 30-day forecasts for each winter season was made because we anticipated that the forcing would not be completely effective in constraining the forced wave components to reproduce those of the analyses (as explained in the previous section), so that the errors in even the forced waves could possibly grow with time. Since a large error in the forced waves would severely compromise the usefulness of the experiments, each winter season was spanned with three overlapping integrations rather than attempting a single seasonal integration.

c. Effectiveness of forcing

In order to confirm that the planetary waves (synoptic waves) were actually being constrained to be close to those in the analysis in the PW (SW) experiments, we examined the correlation between fluctuations of the 300-hPa meridional (v) wind for wavenumbers 0–5 and 6–20 separately. The correlations were computed as functions of forecast time by using deviations from running 11-day means as the input series. For the PW experiments the correlation of wavenumbers 0–5 remains above 0.9 for the entire period, while for the SW experiments the wavenumber 6–20 correlation falls as low as 0.8 in some locations, but is generally above 0.9. There is no indication of a systematic loss of correlation toward the end of the 30-day integrations. A more sensitive measure is the zonally averaged mean-squared error for a single wavenumber. In the appendix, we show that for wavenumbers and latitudes where the SW variance is large, the error is less than about 20% of the analyzed variance, but where the SW variance is small the error can be large, particularly at higher wavenumbers.

d. Error measures

The degree of difference between the analyses and the various experiments is analyzed in terms of a slowly varying component (defined by running 5-day means) and a more rapidly varying component that consists of departures from the former. Our definition of the slowly varying component still allows for the study of the evolution of error within the month. (Error is defined as the difference between any field from one of the GCM integrations and that field from the analyses for the corresponding calendar date.) The 5-day (pentad) mean fields and errors are dominated by the PW scales, while the SW scales tend to be dominated by the high-frequency transients (see Straus and Shukla 1981). The pentad-mean errors are divided into systematic errors, which are defined as errors averaged over all 36 integrations but dependent upon the time relative to the start of the forecast, and random errors, which are mean-squared departures of the errors from the systematic errors, and are also dependent upon the relative forecast time (see the appendix). The errors of the higher frequencies are defined in terms of the high-frequency transient feedback onto the mean flow that is implied by the convergence of the vorticity flux associated with the SW–SW and PW–SW interactions. These vorticity flux convergences (which imply a vorticity, or associated streamfunction tendency) were calculated using the *rotational* component of the flow, as recommended by Hurrell (1995). Details are given in the appendix.

4. Pentad mean errors

a. Systematic error

The systematic error of the 500-hPa height is calculated as function of time for the 26 running pentads for each set of experiments. Northern Hemispheric maps of the systematic error for the control run are given for the pentads starting at forecast days 1, 6, 10, and 26 (final pentad) in Fig. 1. The growth of the systematic error over the first few weeks is not unexpected, and

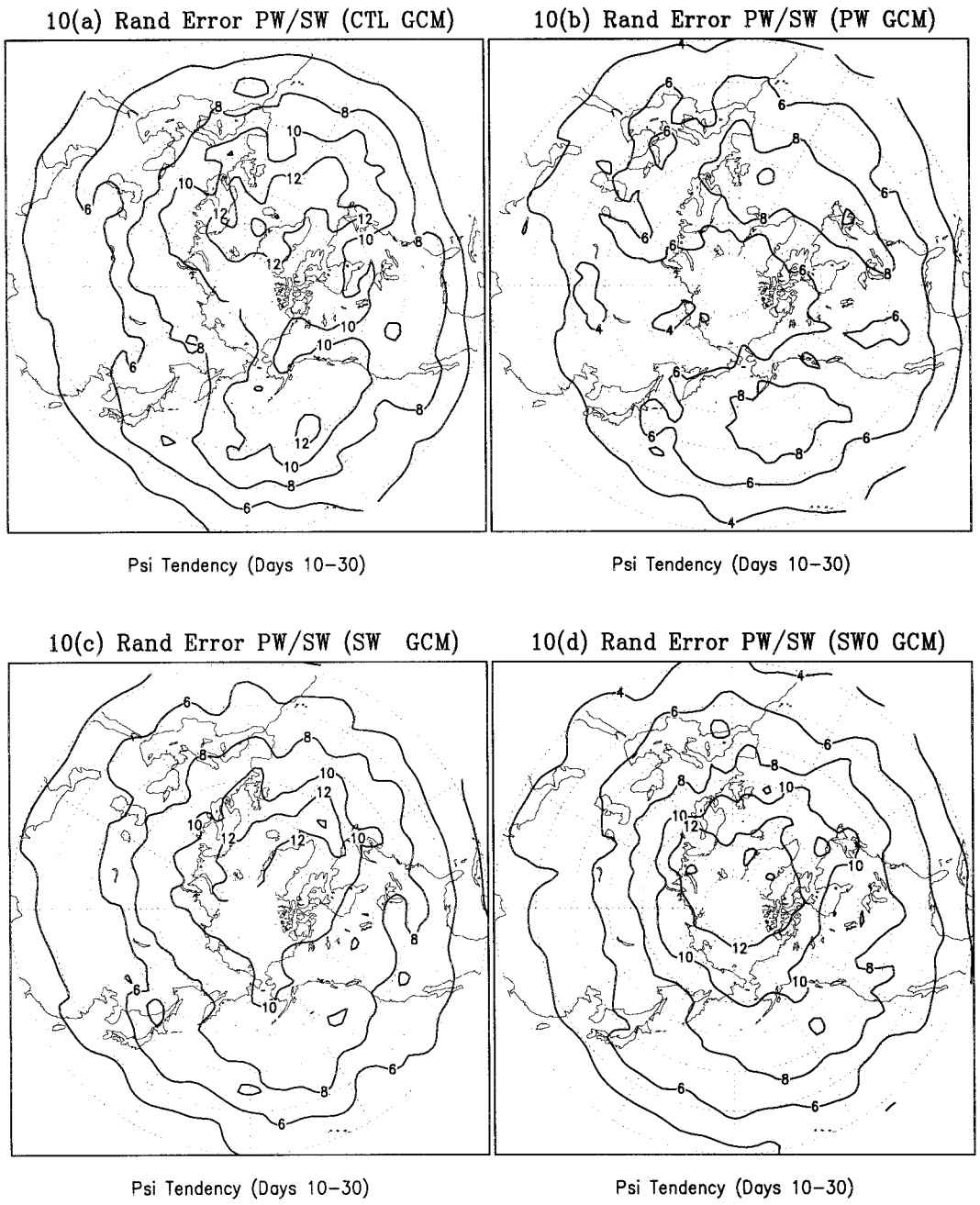

FIG. 10. Random error of 5-day mean streamfunction tendency due to PW–SW transient interactions, vertically integrated, for days 10–30. (a) Control experiment. (b) PW-forced experiment. (c) SW-forced experiment. (d) SW0 forced experiment. (e) SW01-forced experiment. Contour interval is 2.0×10^6 m^2 s^{-1} per pentad.

the pattern that emerges between days 10 and 15 remains fixed, although its magnitude grows. Large negative errors over the northern Atlantic and Pacific Oceans are accompanied by a large positive error over northeastern Canada, indicating the GCM's inability to simulate the trough that is observed at this location. The errors in height gradient over the eastern Pacific Ocean are consistent with an extension of the Pacific jet to the east in the GCM, while the gradient errors over the Atlantic are consistent with an equatorward shift of the jet. Smaller errors are seen at lower latitudes. The systematic error maps for the experiments PW, SW, SW0, and SW01 are shown for the final pentad (days 26–30) in Fig. 2. The PW systematic error is very small, which is a trivial result because 5-day means in general are dominated by the PWs, which are forced from the analyses here. The systematic error of the SW experiment shown in Fig. 2b has a structure very similar to that of

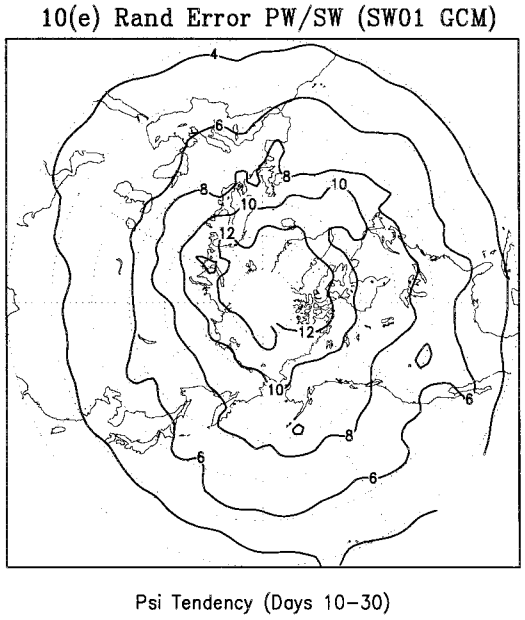

FIG. 10. (*Continued*)

the control, although the magnitude of the extreme errors is smaller, especially over the Atlantic. A fairly large error over central Asia is introduced, however. While the error equatorward of 50°N is further reduced in the SW0 experiment shown in Fig. 2c, the Canadian error is reduced only slightly. This large error is eliminated in the SW01 experiment shown in Fig. 2d, indicating that unless the GCM with realistic SW forcing also has the observed structure in both the zonal flow and wavenumber 1, the large error over Canada cannot be eliminated. Put another way, the systematic error is nearly eliminated[2] in the SW01 run even though wavenumbers 2 through 5 (which are clearly seen as contributors to the systematic error in Figure 1d) evolve freely in the GCM.

The effects of pure synoptic wave forcing on the GCM are further explored in Fig. 3, which shows the zonal mean of the systematic error, plotted as a function of the starting day of the running pentad, for both the SW and control runs. The negative errors that develop in the control run at midlatitudes are exacerbated in the SW experiment, particularly beyond day 15. The error in the zonal mean also appears in the temperature field (not shown), and it is larger at 500 hPa than at either 850 hPa or 200 hPa. It is this additional zonal mean error induced by the SW forcing that motivated the SW0 experiment. The zonal mean of the systematic errors in the PW, SW0, and SW1 experiments (not shown) is very small, indicating that the forcing of this component is very effective.

b. Random error

The square root of the zonal mean of the random error R^2 of running pentad means for 500-hPa height is shown in Fig. 4 for all the experiments. The near vanishing of the PW random error compared to that of the control further indicates the effectiveness of the PW forcing. The error reduction seen in the SW and SW0 experiments is much more modest, with the day 26–30 error at 50°N (for example) decreasing from 140 m (control) to about 110 m in the SW and SW0 experiments. There is a much more substantial reduction in the SW01 experiment, where the random error is only about half that of the control. It is noteworthy that while the systematic error in the SW01 experiment has been almost completely eliminated, this is not true of the random component.

5. Transient errors

a. SW–SW transient interactions

The streamfunction tendency due to the transient SW–SW interactions is shown for the control GCM integrations in Fig. 5a, where it has been averaged over the six pentads corresponding to forecast days 6–10, 11–15, 16–20, 21–25, and 26–30, and further averaged over all 36 control integrations. Thus it is equivalent to the feedback on the monthly mean flow due to the high-frequency transients. Figure 5b shows the corresponding field from the analyses. These diagnostics have been averaged vertically between 850 hPa and 100 hPa, and are reported as a tendency in units of 10^6 m^2 s^{-1} per pentad of time. All the results of this section are presented similarly. Figure 5b indicates the reinforcement of the mean Atlantic and Pacific jets by the transient synoptic wave interaction, whereas in Fig. 5a the feedback by the transients is shifted dramatically eastward in the Pacific, and equatorward in the Atlantic. These errors are similar to the pentad mean errors seen in the previous subsection. The *systematic* error in the SW–SW transient forcing (given by the difference of Figs. 5a and 5b above) is shown in Fig. 6a, along with the errors in the PW, SW, SW0, and SW01 experiments, given in Figs. 6b–e, respectively. The sharp reduction in the systematic error in Figs. 6c–e is due to the effective forcing of the synoptic waves in the corresponding experiments. The almost equal degree of error reduction seen in Fig. 6b comes about solely as a result of planetary wave forcing. It is noteworthy that this PW forcing is as effective in reducing the errors in the region of northeastern Canada as the SW forcing.

The *random* errors in the SW–SW transient forcing are shown in Fig. 7, where they have been averaged over the same pentads as for Fig. 6. (See the appendix

[2] The relatively large negative error over central Asia is probably related to the errors introduced by the vertical interpolation from the pressure surfaces of the analysis to the sigma surfaces of the GCM.

for details of their computation.) Here all the synoptic wave forcing runs, SW, SW0, and SW01, are effective in reducing the random error from the level of the control run in Fig. 7a by nearly a factor of 2. The PW forcing has little effect in reducing the random error, as seen by a comparison of Figs. 7a and 7b.

b. PW–SW transient interactions

The transient interactions between synoptic and planterary waves are reported here in precisely the same format as in section 5a above. Figure 8 shows the associated streamfunction tendency (again averaged over the pentads corresponding to forecast days 10–30) for the control integrations and the analyses. The results from the analyses in Fig. 8b indicate a general reinforcement of the Pacific jet, and some indication of a steering of the Atlantic jet toward the northeast. The GCM errors include a large positive tendency in the eastern Pacific (implying an erroneous meridional wind) and a clear tendency to steer the Atlantic jet in a pure eastward direction. The systematic errors in the PW–SW transient interactions are given for all experiments in Fig. 9 (which is completely analogous to Fig. 6). The reduction of the systematic error here is marginal for the SW run, but is more distinct for the PW and SW01 runs. The random errors are shown in Fig. 10, which is analogous to Fig. 7. While a very modest reduction in the magnitude of the random error is seen in Figs. 10c and 10d, the PW-forced run shows a larger degree of reduction, particularly at high latitudes. The SW01 results show an impressive reduction of the errors over the northern Pacific and Atlantic Oceans.

6. Discussion

In interpreting these results, we try to separate the effects of the GCM bias from the basic interaction properties of the wave groups (SW and PW) in the atmosphere. The large *systematic* errors in the pentad-mean height field from the SW-forced integrations as seen in Figs. 2b and 3b are an indication of errors in the GCM formulation of the PW subsubsystem, for the pentad means shown in Figs. 2 and 3 are dominated by the PWs. These errors, possibly related to the diabatic heating parameterizations, lead to biases in the time-mean, ensemble-mean flow even in the presence of SW forcing taken from analyses. Evidence that the errors in the GCM's PWs strongly involve wavenumbers 0 and 1 is given in Fig. 2d, which shows a dramatic reduction in the mean bias once the zonal flow and wavenumber 1 are correct.

It is possible that the relatively large systematic height error in the SW runs is due either to the inaccuracies in the forcing method, or to the effects of wavenumbers higher than 20. With regard to the first point, the most rapidly developing synoptic waves are those that are most poorly forced in our scheme, and yet they may be responsible for significant mean flow interaction. Yet the systematic error in the synoptic wave transient vorticity flux convergence is quite small in the SW runs, and even the random error of this sensitive quantity is much reduced from that of the control GCM. This indicates a high degree of realism in the forcing of the synoptic waves. (Also see the discussion in the appendix.) With regard to the second point (smaller-scale effects), we have directly calculated the transient vorticity flux convergence of the very small scales (and that due to the interaction of the very small scales with the synoptic and planetary scales) for both the analyses and the GCM, and it is generally much smaller than the contributions involving only the planetary and synoptic waves.

The random component of the pentad-mean height error, shown in Fig. 4, reflects in addition the lack of predictability of the PW system itself. The very modest error reduction seen in Fig. 4c argues that the PW evolution itself is intrinsically chaotic and is not tightly constrained by the SW configuration (Reinhold and Yang 1993).

Evidence that the PW systematic influence on the SWs is generally quite strong is given in Fig. 6. Here the systematic error of the synoptic wave vorticity flux convergence is generally greatly reduced in the SW-forced runs shown in Fig. 5c, as would be expected. However, over the northwestern Atlantic where the systematic (PW) error in the mean height gradient is strong, a large error remains, an error that is not much further reduced by additional constraints on the zonal flow. In contrast, the generally low level of the error in the SW vorticity flux convergence in the PW-forced runs, and the lack of strong localized features, argues both that the PWs very effectively steer the SW activity on average, *and* that the GCM is handling wavenumbers 6–20 in a realistic manner. The former conclusion is in agreement with previous diagnostic work (e.g., Lau 1988), while the latter reinforces the notion that it is the longest waves which are most in error in the GCM. A cautionary note is provided by Fig. 6e, which indicates that the coherent error in SW vorticity flux convergence over the northwestern Atlantic is still noticeable *even in runs which have almost no PW systematic error,* as seen in Fig. 2d. It seems that the (unconstrained) wavenumbers 2–5 in the GCM have nonsystematic errors which nonetheless leave a residual systematic error in the SW configuration.

The level of nonsystematic (random) error in the SW vorticity flux convergence is considerably reduced from the control integrations in all three sets of integrations involving SW, and the extent of the reduction gives a measure of the effectiveness of the forcing. The much larger random error in the PW-forced integrations emphasizes the inherent lack of predictability in the SWs.

The explicit interactions between the PWs and SWs, measured by the sum of PW convergence of SW vorticity and SW convergence of PW vorticity, should be

improved by the specification of either subsystem from analyses. Yet, as shown in Figs. 9 and 10, the systematic error of this transient–mean flow interaction term is lower in the PW experiment than in the SW experiment, and the corresponding random error is also dramatically reduced at high latitudes. Again, the importance of the PW steering of SWs is emphasized.

These results imply a fair degree of control of synoptic wave activity by the planetary waves. They also imply that realistic synoptic wave structures do not by themselves correct systematic errors in the planetary wave mean flow. This is at least consistent with the experience that increasing the horizontal resolution of GCMs beyond a certain point does not yield a more realistic flow (Boyle 1993), even though the higher-resolution models presumably simulate synoptic wave development more accurately.

Very rapidly developing synoptic waves, which may not be captured with complete fidelity by our simple forcing scheme, can play an important role in determining the evolution of the plantery wave structure, particularly those changes connected to regime transitions (Reinhold and Yang 1993). A comprehensive observational study of the synoptic behavior of baroclinic eddies prior to the onset of blocking (Nakamura and Wallace 1993) emphasizes changes that take place over several days. Enhancing the effectiveness of forcing the synoptic waves in GCMs from analyses by a combination of more frequent data insertion and a better forcing scheme awaits the future.

Acknowledgments. We wish to acknowledge useful discussions with Drs. Paul Dirmeyer, Ben Kirtman, and Edwin Schneider. In addition, the comments of the anonymous referees were helpful. This work was supported by National Science Foundation Grant ATM 93-01228.

APPENDIX

Technical Matters

a. Amplitude and phase errors

We develop a simple formalism to define an error measure for the wavenumbers that are forced. For zonal wavenumber m (at a fixed latitude, level and time), we write a particular variable of the GCM T as

$$T = A\cos(m\lambda + \varphi), \tag{A1}$$

where λ is longitude, A the wave amplitude, and φ the wave phase. The corresponding variable T^* for the analyses (toward which the GCM is forced) is given, at the same latitude and time and the same zonal wavenumber, as

$$T^* = A^*\cos(m\lambda + \varphi^*). \tag{A2}$$

The zonal variance of T, namely the value of T^2 averaged around a latitude circle, is just

$$V = \frac{1}{2}T^2. \tag{A3}$$

It is straightforward to show that the zonal variance of the error (GCM minus analysis) can be written as

$$E = \frac{1}{2}\{(A - A^*)^2 + 2AA^*[1 - \cos(\varphi - \varphi^*)]\}$$
$$= E_{\text{AMP}} + E_{\text{PHA}}. \tag{A4}$$

Here E is the mean-squared error, and E_{AMP} and E_{PHA} the components due to errors in the amplitude and phase, respectively.

Figure A1a shows V for the 300-hPa v wind for the analyses, averaged over all analysis times corresponding to forecast day 15 in the SW experiment. The synoptic wave maximum at zonal wavenumber 6 is clear in both hemispheres, while an additional planetary wave maximum is present in the Northern Hemisphere. Figures A1b–d show the errors for the SW-forced experiments. The total error E is shown in Fig. A1b, while E_{AMP} and E_{PHA} are shown in Figs. A1c and A1d, respectively. In all cases the error is normalized by V of Fig. A1a. Note the sharp drop-off in error at wavenumber 6, corresponding to the fact that for the SW experiments only wavenumbers 6–20 are forced. For most latitudes and *synoptic* wavenumbers for which V is large, the errors are modest (below 0.2), giving a measure of the effectiveness of the forcing.

b. Amplitude and phase forcing

We further develop the forcing introduced in section 2a of the paper to examine the phase and amplitude forcing. Equations (A1) and (A2) can be written as

$$T = a\cos(m\lambda) + b\sin(m\lambda) \tag{A5}$$

and

$$T = a^*\cos(m\lambda) + b^*\sin(m\lambda). \tag{A6}$$

In terms of this representation, Eq. (A1) of the paper can be written as

$$\frac{\partial a}{\partial t} = \cdots + \frac{1}{\tau}(a^* - a) \tag{A7}$$

and

$$\frac{\partial b}{\partial t} = \cdots + \frac{1}{\tau}(b^* - b). \tag{A8}$$

In terms of amplitude and phase, the forcing can be expressed as

$$\frac{\partial \varphi}{\partial t} = \cdots - \frac{1}{\tau}\frac{A}{A^*}\sin(\varphi - \varphi^*) \tag{A9}$$

and

$$\frac{\partial A}{\partial t} = \cdots + \frac{1}{\tau}[A^*\cos(\varphi - \varphi^*) - A]. \tag{A10}$$

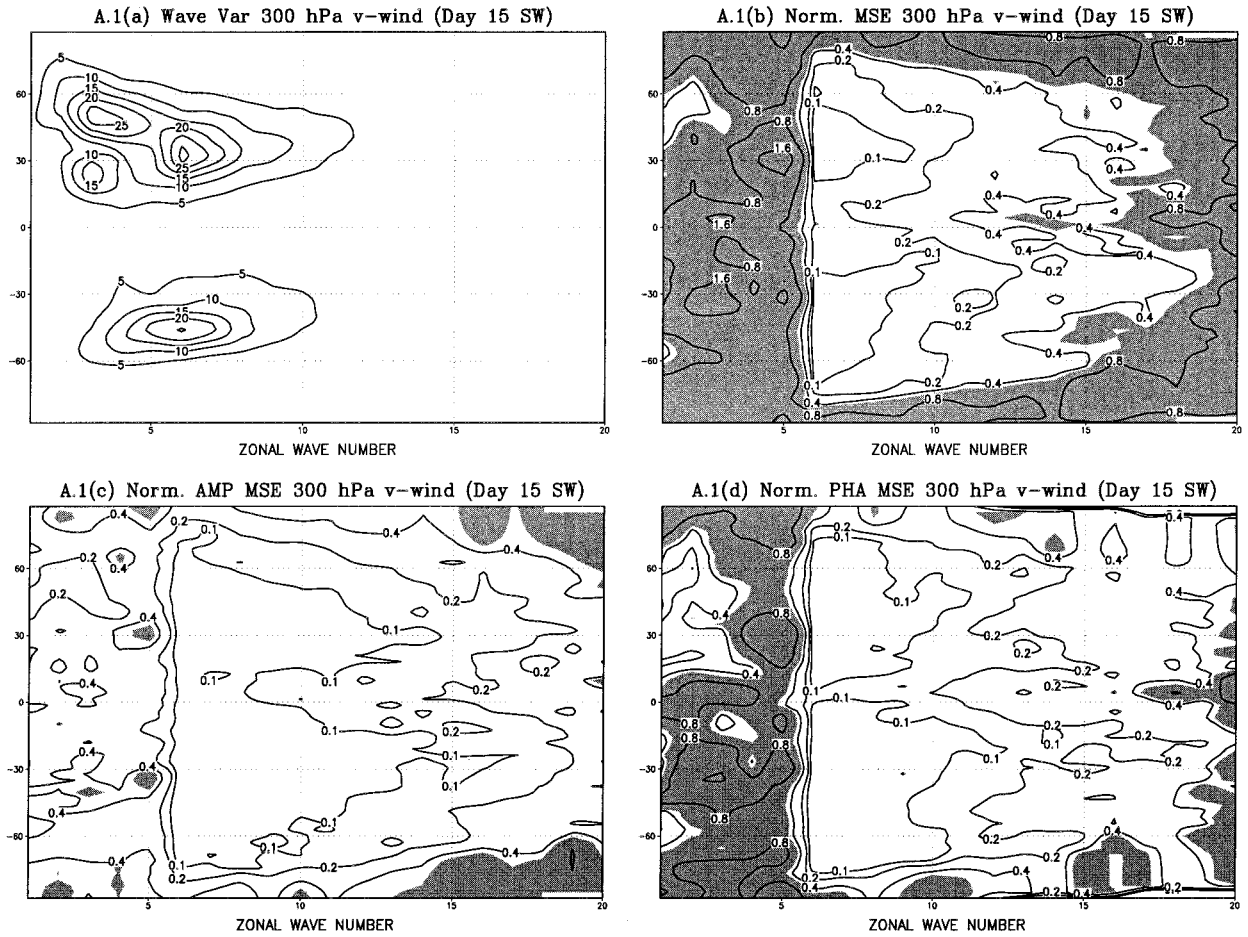

FIG. A1. (a) Zonal variance of 300-hPa v wind at forecast day 15 as a function of zonal wavenumber and latitude. Contour interval is 5 $m^2\ s^{-2}$. (b) Total normalized zonal error variance of 300-hPa v wind at forecast day 15. (c) Normalized zonal error variance of 300-hPa v wind at forecast day 15 due to amplitude errors. (d) Normalized zonal error variance of 300-hPa v wind at forecast day 15 due to phase errors. All panels averaged over the SW experiments. Contour interval is 0.1 for panels (b)–(d). Shading for values greater than 0.5.

The simulated amplitude and phases are not uniformly forced toward the target amplitude and phase indicated by the asterisks. In particular, errors in the phase of the simulated wave can cause the amplitude to be forced incorrectly. An extreme case occurs when the simulated wave is perfectly out of phase with the forced wave, in which case the amplitude forcing is negative and the simulated wave decays.

The amplitude and phase A and φ are related to the coefficients a and b:

$$A^2 = (a^2 + b^2) \tag{A11}$$

and

$$\mathcal{T} = \tan(\varphi) = -\frac{b}{a}. \tag{A12}$$

We introduce more general forcing for the components a and b in the form

$$\frac{\partial a}{\partial t} = \cdots + \frac{1}{\tau}(F_a - a) \tag{A13}$$

and

$$\frac{\partial b}{\partial t} = \cdots + \frac{1}{\tau}(F_b - b), \tag{A14}$$

where F_a and F_b are to be chosen. The corresponding forcing of A^2 and $\mathcal{T}$ can be written as

$$2A\frac{\partial A}{\partial t} = a\frac{\partial a}{\partial t} + b\frac{\partial b}{\partial t} = \cdots + \frac{1}{\tau}(aF_a + bF_b - A^2) \tag{A15}$$

and

$$\frac{\partial \mathcal{T}}{\partial t} = -\frac{b}{a^2}\frac{\partial a}{\partial t} - \frac{1}{a}\frac{\partial b}{\partial t} \cdots + \frac{2}{\tau}\left[\left(-\frac{b}{2a^2}F_a - \frac{1}{2a}F_b\right) - \mathcal{T}\right]. \tag{A16}$$

Equations (A15) and (A16) have the desired form of directly forcing the amplitude squared A^2 and phase tangent $\mathcal{T}$ if F_a and F_b satisfy

$$aF_a + bF_b = A^{*2} \tag{A17}$$

and

$$-bF_a - aF_b = 2\mathcal{T}^* a^2, \tag{A18}$$

where $\mathcal{T}^* = \tan(\varphi^*)$. The solutions to Eqs. (A17) and (A18) are

$$F_a = \frac{aA^{*2} + 2\mathcal{T}^* a^2 b}{a^2 - b^2} \tag{A19}$$

and

$$F_b = \frac{bA^{*2} + 2\mathcal{T}^* a^3}{b^2 - a^2}, \tag{A20}$$

which, while linear in the squared amplitude and phase tangent of the target wave, are nonlinear and possibly singular in the original GCM wave variables.

c. Systematic and random errors

Let $x_{i,j}$ denote the ith running 5-day (pentad) mean of the GCM predicted quantity x from forecast j. Note that $x \le i \le 26$ since the forecasts are 30 days long. The forecast label j can be thought of as a label of the initial conditions, of which there are $N = 36$ for each GCM configuration, corresponding to 12 winters and three initial dates (15 December, 1 January, 15 January) for each winter. Let the analysis value of the same quantity be $X_{i,j}$.

The systematic error S_i is then defined as

$$S_i = \frac{1}{N}\sum_j (x_{i,j} - X_{i,j}) \tag{A21}$$

and the squared random error R_i^2 is defined as

$$R_i^2 = \frac{1}{N}\sum_j (x_{i,j} - X_{i,j} - S_i)^2. \tag{A22}$$

In section 4 of the paper, x and X refer to 500-hPa height, while in section 5 they refer to the convergence of transient vorticity flux. In each section, it is S_i and R_i which are plotted.

d. Transient vorticity flux convergence

The transient vorticity flux convergence is computed by first removing the (running) pentad mean vorticity from the total vorticity. Call the transient deviation ζ'. This is partitioned into planetary wave (PW), synoptic wave (SW), and small-scale (XW) components on the basis of zonal wavenumber m alone, corresponding to $(0 \le m \le 5)$, $(6 \le m \le 20)$, and $21 \le m$, respectively:

$$\zeta = \zeta'_{\rm PW} + \zeta'_{\rm SW} + \zeta'_{\rm XW}. \tag{A23}$$

Let $\mathbf{v}'_{\rm PW}$, $\mathbf{v}'_{\rm SW}$, and $\mathbf{v}'_{\rm XW}$ be the nondivergent velocity fields corresponding to $\zeta'_{\rm PW}$, $\zeta'_{\rm SW}$, and $\zeta'_{\rm XW}$. The contribution of the rotational vorticity flux convergence to the total pentad vorticity budget can be written as

$$\frac{\partial \overline{\zeta}}{\partial t} = -\boldsymbol{\nabla}\cdot\overline{(\mathbf{v}'\zeta')} - \boldsymbol{\nabla}\cdot(\overline{\mathbf{v}}\,\overline{\zeta}), \tag{A24}$$

where the overbars denote pentad mean. The first term on the right-hand side gives the contribution of the transients, and can be written as

$$-\boldsymbol{\nabla}\cdot\overline{(\mathbf{v}'\zeta')} = -[\boldsymbol{\nabla}\cdot\overline{(\mathbf{v}'_{\rm PW}\zeta'_{\rm SW})} + \boldsymbol{\nabla}\cdot\overline{(\mathbf{v}'_{\rm SW}\zeta'_{\rm PW})}] - + \boldsymbol{\nabla}\cdot\overline{(\mathbf{v}'_{\rm SW}\zeta'_{\rm SW})} - \cdots, \tag{A25}$$

where the XW terms are not written explicitly. The two terms grouped in square brackets are referred to as the PW–SW interactions, and the third term as the SW–SW interactions. In the paper these are reported as streamfunction tendencies, obtained from the above vorticity tendencies by application of the inverse Laplacian operator.

REFERENCES

Benzi, R., P. Malguzzi, A. Speranza, and A. Sutera, 1986a: The statistical properties of the general atmospheric circulation: Observational evidence and a minimal theory of bimodality. *Quart. J. Roy. Meteor. Soc.*, **112,** 661–674.

——, A. Speranza, and A. Sutera, 1986b: A miminmum baroclinic model for the statistical properties of low-frequency variability. *J. Atmos. Sci.*, **43,** 2962–2967.

Blackmon, M. L., and G. H. White, 1982: Zonal wavenumber characteristics of Northern Hemisphere transient eddies. *J. Atmos. Sci.*, **39,** 1985–1998.

Bloom. S. C., L. L. Takacs, A. M. daSilva, and D. Ledvina, 1996: Data assimilation using incremental analysis updates. *Mon. Wea. Rev.*, **124,** 1256–1271.

Boer, G. J., and T. G. Shepherd, 1983: Large-scale two-dimensional turbulence in the atmosphere. *J. Atmos. Sci.*, **40,** 164–184.

Boyle, J. S., 1993: Sensitivity of dynamical quantities to horizontal resolution for a climate simulation using the ECMWF (cycle 33) model. *J. Climate*, **6,** 796–815.

Branstator, G., 1992: The maintenance of low-frequency atmospheric anomalies. *J. Atmos. Sci.*, **49,** 1924–1945.

Charney, J. G., and J. G. deVore, 1979: Multiple flow equilibria in the atmosphere and blocking. *J. Atmos. Sci.*, **36,** 1205–1216.

——, and D. M. Straus, 1980: Form-drag instability, multiple equilibria and propagating planetary waves in baroclinic, orographically forced, planetary wave systems. *J. Atmos. Sci.*, **37,** 1157–1176.

Cheng, X., and J. M. Wallace, 1993: Cluster analysis of the Northern Hemisphere wintertime 500-hPa height field: Spatial patterns. *J. Atmos. Sci.*, **50,** 2674–2696.

Colucci, S. J., 1985: Explosive cyclogenesis and large-scale circulation changes: Implications for atmospheric blocking. *J. Atmos. Sci.*, **42,** 2701–2717.

——, 1987: Comparative diagnosis of blocking versus nonblocking planetary-scale changes during synoptic-scale cyclogenesis. *J. Atmos. Sci.*, **44,** 124–139.

Daley, R., 1991: *Atmospheric Data Analysis.* Cambridge University Press, 457 pp.

Davies, H. C., and R. E. Turner, 1977: Updating prediction models by dynamical relaxation: An examination of the technique. *Quart. J. Roy. Meteor. Soc.*, **103,** 225–245.

de Weaver, E., and S. Nigam, 1997: Dynamics of zonal-mean flow assimilation and implications for winter circulation anomalies. *J. Atmos. Sci.*, **54,** 1758–1775.

Dole, R. M., and N. D. Gordon, 1983: Persistent anomalies of the extratropical Northern Hemisphere wintertime circulation: Geographical distribution and regional persistence characteristics. *Mon. Wea. Rev.,* **111,** 1567–1586.

Egger, J., and H.-D. Schilling, 1983: On the theory of the long-term variability of the atmosphere. *J. Atmos. Sci.,* **40,** 1073–1085.

Ferranti, L., T. N. Palmer, F. Molteni, and E. Klinker, 1990: Tropical-extratropical interaction associated with the 30–60 day oscillation and its impact on medium and extended range prediction. *J. Atmos. Sci.,* **47,** 2177–2199.

Frederiksen, J. S., 1982: A unified three-dimensional instability theory of the onset of blocking and cyclogenesis. *J. Atmos. Sci.,* **39,** 969–987.

Haines, K., and J. Marshall, 1987: Eddy-forced coherent structures as a prototype of atmospheric blocking. *Quart. J. Roy. Meteor. Soc.,* **113,** 681–704.

Hansen, A. R., and A. Sutera, 1986: On the probability density distribution of planetary-scale atmospheric wave amplitude. *J. Atmos. Sci.,* **43,** 3250–3265.

Held, I. M., S. W. Lyons, and S. Nigam, 1989: Transients and the extratropical response to El Niño. *J. Atmos. Sci.,* **46,** 163–174.

Horel, J. D., 1981: A rotated principal component analysis of the interannual variability of the Northern Hemisphere 500 mb height field. *Mon. Wea. Rev.,* **109,** 2080–2092.

Hoskins, B. J., and D. J. Karoly, 1981: The steady linear response of a spherical atmosphere to thermal and orographic forcing. *J. Atmos. Sci.,* **38,** 1179–1196.

Hurrell, J. W., 1995: Transient eddy forcing of the rotational flow during northern winter. *J. Atmos. Sci.,* **52,** 2286–2301.

Kalnay, E., and Coauthors, 1996: The NCEP/NCAR 40-year/reanalysis project. *Bull. Amer. Meteor. Soc.,* **77,** 437–472.

Kimoto, M., and M. Ghil, 1993: Multiple flow regimes in the Northern Hemisphere winter. Part I: Methodology and hemispheric regimes. *J. Atmos. Sci.,* **50,** 2625–2643.

Klinker, E., 1990: Investigation of systematic errors by relaxation experiments. *Quart. J. Roy. Meteor. Soc.,* **116,** 573–194.

Krishnamurthi, T. N., H. S. Bedi, W. Heckley, and K. Ingles, 1988: Reduction of the spinup time for evaporation and precipitation in a spectral model. *Mon. Wea. Rev.,* **116,** 907–920.

Kung, E. C., and W. E. Baker, 1986: Spectral energetics of the observed and simulated Northern Hemisphere general circulation during blocking episodes. *J. Atmos. Sci.,* **43,** 2792–2812.

Kushnir, Y., and J. M. Wallace, 1989: Interaction of low- and high-frequency transients in a forecast experiment with a general circulation model. *J. Atmos. Sci.,* **46,** 1411–1418.

Lau, N.-C., 1988: Variability of the observed midlatitude storm tracks in relation to low-frequency changes in the circulation pattern. *J. Atmos. Sci.,* **45,** 2718–2743.

Legras, B., and M. Ghil, 1985: Persistent anomalies, blocking and variations in atmospheric predictability. *J. Atmos. Sci.,* **42,** 433–471.

Macpherson, B., 1991: Dynamic initialization by repeated insertion of data. *Quart. J. Roy. Meteor. Soc.* **117,** 965–991.

Miyakoda, K., J. Sirutis, and J. Ploshay, 1986: One-month forecast experiments—Without anomaly boundary forcings. *Mon. Wea. Rev.,* **114,** 2363–2401.

Molteni, F., and S. Tibaldi, 1990: Regimes in the wintertime circulation over northern extratropics. II: Consequences for dynamical predictability. *Quart. J. Roy. Meteor. Soc.,* **116,** 1263–1288.

——, and T. N. Palmer, 1991: A real-time scheme for the prediction of forecast skill. *Mon. Wea. Rev.,* **119,** 1088–1097.

——, S. Tibaldi, and T. N. Palmer, 1990: Regimes in the wintertime circulation over northern extratropics. I: Observational evidence. *Quart. J. Roy. Meteor. Soc.,* **116,** 31–68.

Nakamura, H., and J. M. Wallace, 1991: Skewness of low-frequency fluctuations in the tropospheric circulation during Northern Hemisphere winter. *J. Atmos. Sci.,* **48,** 1441–1448.

——, and ——, 1993: Synoptic behavior of baroclinic eddies during blocking onset. *Mon. Wea. Rev.,* **121,** 1892–1903.

O'Lenic, E., and R. Livezey, 1989: Relationships between low-frequency anomalies and systematic errors in medium- and extended-range forecasts. *Mon. Wea. Rev.,* **117,** 1262–1280.

Palmer, T. N., 1988: Medium and extended range predictability and the stability of the Pacific/North American Mode. *Quart. J. Roy. Meteor. Soc.,* **114,** 691–713.

——, C. Branković, F. Molteni, and S. Tibaldi, 1990: Extended-range predictions with ECMWF models: Interannual variability in operational model integrations. *Quart. J. Roy. Meteor. Soc.,* **116,** 799–834.

Rambaldi, S., and K. C. Mo, 1984: Forced stationary solutions in a barotropic channel: Multiple equilibria and the theory of nonlinear resonance. *J. Atmos. Sci.,* **41,** 3135–3146.

Reinhold, B. B., and R. J. Pierrehumbert, 1982: Dynamics of weather regimes: Quasi-stationary waves and blocking. *Mon. Wea. Rev.,* **110,** 1105–1145.

——, and S. Yang, 1993: The role of transients in weather regimes and transitions. *J. Atmos. Sci.,* **50,** 1173–1180.

Simmons, A. J., and B. J. Hoskins, 1978: The life cycles of some nonlinear baroclinic waves. *J. Atmos. Sci.,* **35,** 414–442.

——, J. M. Wallace, and G. W. Branstator, 1983: Barotropic wave propagation and instability, and atmospheric teleconnection patterns. *J. Atmos. Sci.,* **40,** 1363–1391.

Straus. D. M., and J. Shukla, 1981: Space-time spectral structure of a GLAS general circulation model and a comparison with observations. *J. Atmos. Sci.,* **38,** 902–917.

Tanaka, H. L., 1991: A numerical simulation of amplification of low-frequency planetary waves and blocking formations by the upscale energy cascade. *Mon. Wea. Rev.,* **119,** 2919–2935.

Tibaldi, S., and F. Molteni, 1990: On the operational predictability of blocking. *Tellus,* **42A,** 343–365.

Tracton M. S., 1990: Predictability and its relationship to scale interaction processes in blocking. *Mon. Wea. Rev.,* **118,** 1666–1695.

——, K. Mo, W. Chen, E. Kalnay, R. Kistler, and G. White, 1989: Dynamical extended range forecasting (DERF) at the National Meteorological Center. *Mon. Wea. Rev.,* **117,** 1604–1635.

Vautard, R., and B. Legras, 1988: On the source of mid-latitude low frequency variability. Part II: Nonlinear equilibration of weather regimes. *J. Atmos. Sci.,* **45,** 2845–2867.

Wallace, J. M., and D. S. Gutzler, 1981: Teleconnections in the geopotential height field during the Northern Hemisphere winter. *Mon. Wea. Rev.,* **109,** 784–812.

Xue, Y., M. J. Fennessy, and P. J. Sellers, 1996: Impact of vegetation properties on U.S. summer weather prediction. *J. Geophys. Res.,* **101D,** 7419–7430.